



**Experimental determination of the diffusion coefficient in a coated cell**Junhe Zheng, Ekrem Abdukerim, Baichuan Li , Teng Wu ,\* and Hong Guo<sup>†</sup>*State Key Laboratory of Advanced Optical Communication Systems and Networks, School of Electronics, and Center for Quantum Information Technology, Peking University, Beijing 100871, China*

(Received 19 February 2024; revised 3 May 2024; accepted 5 June 2024; published 24 June 2024)

The motional averaging effect of the alkali-metal atoms in a coated cell is influenced by the non-negligible background gas and is characterized by the diffusion coefficient of the alkali-metal atoms. In this paper, we present an experimental approach to measure the atomic diffusion coefficient within a paraffin coated cell through analyzing the spin relaxation caused by first-order and second-order magnetic-field gradients, respectively, given the distinct dependencies of these two relaxation effects on the diffusion coefficient. The diffusion coefficient is measured to be  $0.137 \text{ m}^2/\text{s}$  for the fabricated paraffin coated cell, indicating an estimated pressure of background gas at approximately  $0.25 \text{ Pa}$ , which is orders of magnitude higher than the typical saturated vapor pressure of the alkali-metal atoms. Our work serves as a potential nondestructive method for analyzing the background gas pressure and offers new insights into the performance characterization of the coated cell.

DOI: [10.1103/PhysRevA.109.062814](https://doi.org/10.1103/PhysRevA.109.062814)**I. INTRODUCTION**

Polarized alkali-metal atoms inside a cell with antirelaxation coating can undergo thousands of collisions with the wall surface without losing polarization, resulting in a long relaxation time [1–3]. Such an advantage has propelled the alkali-metal vapor cell with antirelaxation coating to play a remarkable role in widespread applications [4–7]. Furthermore, in a buffer-gas-free coated cell, the low pressure allows alkali-metal atoms to rapidly sample the overall volume of the cell, thereby averaging the magnetic field over the relaxation time [8]. This characteristic constitutes another advantage of the coated cell, called the motional averaging effect, which suppresses the relaxation effect induced by magnetic-field gradient [9,10] and has been utilized in various studies [11,12]. The motional averaging effect is closely related to the atomic motional characteristics. With the consideration of low saturated alkali-metal atomic vapor pressure, the mean free path of atoms inside the coated cell is significantly larger than the cell size. As a result, the atoms travel ballistically between adjacent atom-wall collisions [13,14], leading to a strong suppression of magnetic-field-gradient-induced relaxation [15,16].

Nevertheless, under certain conditions, the atomic motional characteristics within the coated cell do not exhibit ideal ballistic motion. Due to chemical reactions of alkali-metal atoms with the coating, resulting in outgassing, the existence of non-negligible background gas is not an occasional phenomenon in the coated cell [17–22]. It has been reported that the pressure of background gas ( $\sim 1 \text{ Pa}$ ) is much larger than the saturated vapor pressure of alkali-metal atoms [23,24]. Consequently, atoms no longer travel ballistically between

the adjacent atom-wall collisions, leading to suppression of atomic motion and degradation of the motional averaging effect. The diffusion coefficient of alkali-metal atoms in the background gas is an essential parameter for analyzing the atomic motional characteristics inside the coated cell. Therefore, a precise measurement of the diffusion coefficient is important for accurately estimating the performance of the coated cell.

The determination of the diffusion coefficient can be achieved by analyzing spin-polarization relaxation caused by a magnetic-field gradient and can be dated back to the early 1950s. The diffusion of particles is initially taken into consideration in the spin-echo experiment and the impact of diffusion on magnetic-field-gradient-induced spin relaxation is explicitly described by Hahn [25]. The related spin-echo method is developed and becomes an effective approach to measure the diffusion coefficient [26], particularly in the case of the liquid molecular samples with very small diffusion coefficients ( $\sim 10^{-5} \text{ cm}^2/\text{s}$ ) [27–29] and alkali-metal atomic cells with high-pressure buffer gas [30–32].

However, in the case of the coated cell, even when considering the presence of background gas, the diffusion coefficient of alkali-metal atoms is typically much larger than the values of the examples mentioned above [33]. The much larger diffusion coefficient requires precise control of considerably shorter pulse intervals and shorter pulse widths, compared to previous works in the spin-echo method [27–32]. Such a necessity makes it a complex and challenging task to measure the diffusion coefficient of alkali-metal atoms in the coated cell through using the spin-echo method.

Torrey proposes an alternative description for the influence of diffusion on magnetic-field-gradient-induced relaxation [34], which combines the normal diffusion equation with the Bloch equation and gives results similar to those obtained in earlier spin-echo experiments [25,26]. Taking it a step further, Torrey's method is extended by the perturbative theory

\*Contact author: [wuteng@pku.edu.cn](mailto:wuteng@pku.edu.cn)†Contact author: [hongguo@pku.edu.cn](mailto:hongguo@pku.edu.cn)

and is applied to study the magnetic-field-gradient-induced spin relaxation with the consideration of boundaries [35]. In Ref. [36], an equivalent approach combines the Redfield theory and normal diffusion equation, yielding the same results as in Ref. [35]. These methods establish a relation between the magnetic-field-gradient-induced relaxation and the diffusion coefficient and then are applied to measure the diffusion coefficients of noble gases [37–40] and the atomic cell filled with high-pressure buffer gas [41].

Notably, the analysis methods mentioned above are only applicable to cells with high-pressure gas, where the mean free path of atoms is much smaller than the cell size ( $\lambda \ll R$ ) [42]. For the coated cell, the mean free path of atoms may be comparable to or even larger than the cell size. Under such conditions, the normal diffusion equation is not valid and a modified theory should be applied to analyze magnetic-field-gradient-induced relaxation in the coated cell [43]. References [24] and [33] investigate the alkali-metal atomic diffusion in the presence of background gas by measuring the velocity-changing collisions rate and spin-noise spectrum in the coated cell, respectively. Besides, the majority of previous research on analyzing background gas inside the coated cell are typically destructive and rely on a mass spectrometer for analysis [20–23].

In this paper, we present a method for promptly analyzing the atomic diffusion coefficient and a potential nondestructive method to obtain the background gas pressure inside the coated cell. The Redfield theory combined with Langevin's diffusion equation is applied to theoretically analyze the magnetic-field-gradient-induced relaxation in the coated cell. We experimentally obtain the diffusion coefficient of potassium atoms in a fabricated cylindrical paraffin-coated cell, along with the corresponding uncertainty, by measuring and analyzing the transverse spin relaxation caused by first-order and second-order magnetic-field gradients, respectively, given the different dependencies of these two different relaxation effects on the diffusion coefficient. Although the diffusion coefficients obtained under the two magnetic-field gradients exhibit some deviation, we show in detail how to perform error analysis and determine that such a deviation is dominantly attributed to the estimated error of the cell position.

## II. THEORY

This section presents a basic theoretical model for depicting the magnetic-field-gradient-induced spin relaxation in a coated cell. The theoretical model combines the Redfield theory with Langevin's diffusion equation [43]. Additionally, this section outlines the fundamental procedures for determining the diffusion coefficient based on the analysis of magnetic-field-gradient-induced relaxation.

In general, the magnetic-field-gradient-induced spin relaxation is described by the Redfield theory, which is a generalized treatment of second-order time-dependent perturbation [44,45]. Redfield theory has been applied to analyze the magnetic-field-gradient-induced spin relaxation for the cell filled with noble gas [36]. It has also been proved that this approach is equivalent to the theory based on Torrey's diffusion equation with perturbative theory [35,42].

To utilize the Redfield theory for analyzing magnetic-field-gradient-induced relaxation in the coated cell, it is necessary to analyze the characteristic of atomic motion within the cell. The atomic motion can be represented by the conditional probability density, denoted as  $\rho(\vec{r}, t | \vec{r}_0, t_0)$ , which indicates the conditional probability density of an atom being at position  $\vec{r}$  at time  $t$ , given that its initial time and position are  $t_0$  and  $\vec{r}_0$ , respectively. For an atomic vapor cell filled with high-pressure gas, in which the mean free path of the atoms is much smaller than the size of cell ( $\lambda \ll R$ ), the atomic motion can be described by the normal diffusion equation [36]

$$\frac{\partial}{\partial t} \rho(\vec{r}, t | \vec{r}_0, t_0) = D \nabla^2 \rho(\vec{r}, t | \vec{r}_0, t_0), \quad (1)$$

where  $D$  is the diffusion coefficient. Nevertheless, in the case of a coated cell with non-negligible background gas, where the mean free path of atoms is comparable to the size of the coated cell, our previous research suggests that Langevin's diffusion model is more appropriate for describing the atomic motion [43]

$$\frac{\partial}{\partial t} \rho(\vec{r}, t | \vec{r}_0, t_0) = D \left( 1 - e^{-\frac{|t-t_0|}{\tau_D}} \right) \nabla^2 \rho(\vec{r}, t | \vec{r}_0, t_0), \quad (2)$$

where  $\tau_D = Dm/(k_B T)$ , in which  $m$  is the mass of a single atom,  $T$  is the temperature of the cell, and  $k_B$  is the Boltzmann constant. To solve Eq. (2), the boundary condition is assumed to have the form

$$\vec{n} \cdot \frac{\partial \rho(\vec{r}, t | \vec{r}_0, t_0)}{\partial n} \Big|_{r=R} = 0, \quad (3)$$

where  $\vec{n}$  is an outwardly directed normal unit vector to the spherical wall. Equation (3) is known as the Neumann boundary condition and is suitable for high-quality coated cells, i.e., the wall-induced spin relaxation is neglected and the spin relaxation time is much longer than the atomic motional time between adjacent wall collisions [46,47]. The relaxation caused by the magnetic-field gradient can thus be determined by combining the Redfield theory with Langevin's diffusion equation. Detailed derivations can be seen in Appendix A 2. The magnetic-field-gradient-induced spin relaxation is closely associated with the motional characteristics of atoms in the coated cell, i.e., the diffusion coefficient. Thus measuring the magnetic-field-gradient-induced relaxation allows for the determination of the diffusion coefficient  $D$  of the atoms within the coated cell. For a cylindrical coated cell with its axis perpendicular to the  $z$  axis (the direction of the bias magnetic field), as detailed in Appendix A 2, the transverse relaxation time  $T_2$  caused by first-order magnetic-field gradient  $\partial B_z / \partial z$  and second-order magnetic-field gradient  $\partial^2 B_z / \partial z^2$  are given by

$$\frac{1}{\pi T_2} = \frac{\gamma^2}{\pi} W(R, L, D) \times \left( \frac{\partial B_z}{\partial z} \right)^2 = a_1 \times \left( \frac{\partial B_z}{\partial z} \right)^2 \quad (4)$$

and

$$\frac{1}{\pi T_2} = \frac{\gamma^2}{\pi} P(R, L, D) \times \left( \frac{\partial^2 B_z}{\partial z^2} \right)^2 = a_2 \times \left( \frac{\partial^2 B_z}{\partial z^2} \right)^2, \quad (5)$$

where  $R$  and  $L$  represent the radius and length of the cylindrical coated cell, respectively. The terms  $W(R, L, D)$  and  $P(R, L, D)$  are the comprehensive functions that depend on

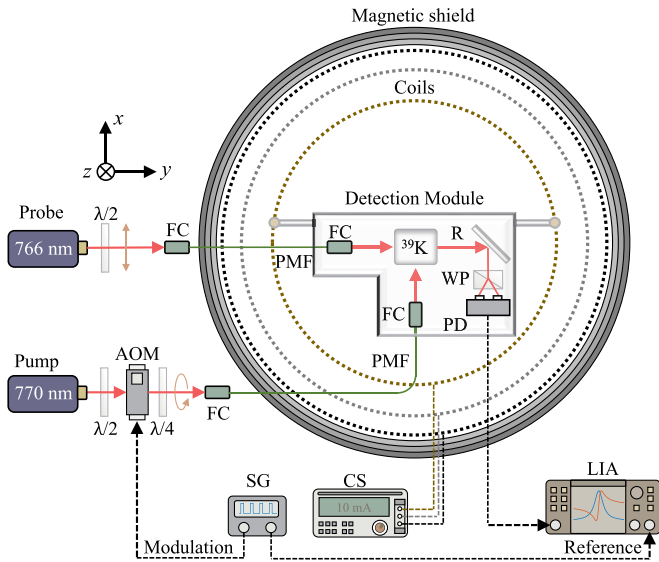


FIG. 1. Experimental setup of an all-optical potassium atomic magnetometer for measuring the magnetic-field-gradient-induced spin relaxation. FC, fiber coupler; PMF, polarization-maintaining fiber;  $\lambda/2$ , half-wave plate;  $\lambda/4$ , quarter-wave plate; WP, Wollaston prism; R, reflector; AOM, acousto-optic modulator; PD, photodetector; LIA, lock-in amplifier; SG, signal generator; CS, current sources. The dashed circles represent the coils, including the nonmoment coil (black), the second-order gradient coil (gray), and the first-order magnetic-field-gradient coil (brown).

both the cell size and the diffusion coefficient. Detailed calculations are provided in Appendixes A 2 c and A 2 d. Besides, it should be noted that the proposed theoretical model is applicable for different cell shapes [43].

The transverse relaxation demonstrates a quadratic relation with both  $\partial B_z/\partial z$  and  $\partial^2 B_z/\partial z^2$  and the corresponding quadratic coefficients are denoted as  $a_1$  and  $a_2$ , which are related to  $D$ . Furthermore, the ratio  $a_1/a_2$  remains a function of  $D$ , as is shown in Appendixes A 2 c and A 2 d. This indicates that the two functions  $a_1$  and  $a_2$  are linearly independent [48]. Consequently, the diffusion coefficient can be independently assessed by measuring the transverse spin relaxation caused by first-order and second-order magnetic-field gradients, respectively.

### III. EXPERIMENT

In this section, an all-optical atomic magnetometer is applied to measure the transverse spin relaxation caused by first-order and second-order magnetic-field gradients, respectively, within a cylindrical paraffin-coated cell. The corresponding diffusion coefficients are determined by combining the experimental results with the proposed theory in Sec. II.

#### A. Apparatus

An all-optical potassium atomic magnetometer based on the Bell-Bloom configuration is schematically shown in Fig. 1 [49]. The  $^{39}\text{K}$  atomic vapor cell coated with paraffin is cylindrical with a radius of  $R = 12.65$  mm and a length of

$L = 30$  mm. The coated vapor cell is heated and maintained at a temperature of  $58.8^\circ\text{C}$  to enhance the signal-to-noise ratio of magnetic resonances.

A circularly polarized pump laser, which is tuned to be resonant with the potassium D1 line, is applied to optically pump the transverse spin polarization along the  $x$  axis. The power of the pump laser is modulated with a 10% duty cycle to drive the spin precession synchronously, if the modulation frequency is close to the spin precession frequency under the axial bias magnetic field  $B_0$ . A linearly polarized laser ( $\sim 200$  MHz blue detuned from the D2 line of the potassium) propagating along the  $y$  axis is used to measure the transverse spin polarization through an optical rotation effect [50]. The power of both lasers entering the vapor cell is less than  $100 \mu\text{W}$ . Polarization-maintaining fibers and fiber couplers are applied to transmit the laser beams into the four-layer magnetic shield. All optical components inside the magnetic shield are nonmagnetic. The coated cell, relevant optical components, and a photodetector are integrated into a detection module made of polyetheretherketone (PEEK).

The coils inside the magnetic shield are driven with the current sources. A nonmoment coil generates the bias magnetic field  $B_0$  along the  $z$  axis (aligned with the axial direction of the magnetic shield and perpendicular to the propagation direction of both the pump beam and the probe beam). Additionally, two magnetic-field-gradient coils are used to independently generate the first-order and second-order axial magnetic-field gradients, i.e.,  $\partial B_z/\partial z$  and  $\partial^2 B_z/\partial z^2$ . The central axes of the magnetic shield and the coils are aligned through manual adjustments. The detection module and first-order gradient coil are fixed together and the cell is positioned at the center of the first-order gradient coil.

The optical rotation signal is measured with a photodetector and is demodulated with a lock-in amplifier (Stanford Research Systems, SR865A). The magnetic resonance is recorded as a function of modulation frequency and a Lorentzian function is utilized for the fitting of magnetic resonance, facilitating the extraction of the signal linewidth [full width at half maximum (FWHM)], as detailed in Appendix B 1. In our experiment, the relation between the linewidth of magnetic resonance and the transverse relaxation time  $T_2$  takes the form of  $\text{FWHM} = 1/(\pi T_2)$ , with the unit Hz. This is a general expression for analyzing the linewidth of magnetic resonance. The primary contributions to transverse spin relaxation include three main factors: wall relaxation, optical power broadening, and magnetic-field gradient. Our work primarily focuses on the transverse spin relaxation caused by the magnetic-field gradient through examining the relation between the magnetic-field gradient and the linewidth of magnetic resonance.

#### B. Magnetic-field-gradient-induced relaxation

To analyze the magnetic-field-gradient-induced transverse spin relaxation, the linewidths of magnetic resonances are recorded under different first-order and second-order magnetic-field gradients, respectively. The bias magnetic field is adjusted as  $B_0 \approx 1200$  nT. Under this condition, the corresponding Larmor frequency satisfies the condition  $\omega_0 \gg D/R^2$ , allowing one to disregard the influence of  $T_1$  on  $T_2$  [43].

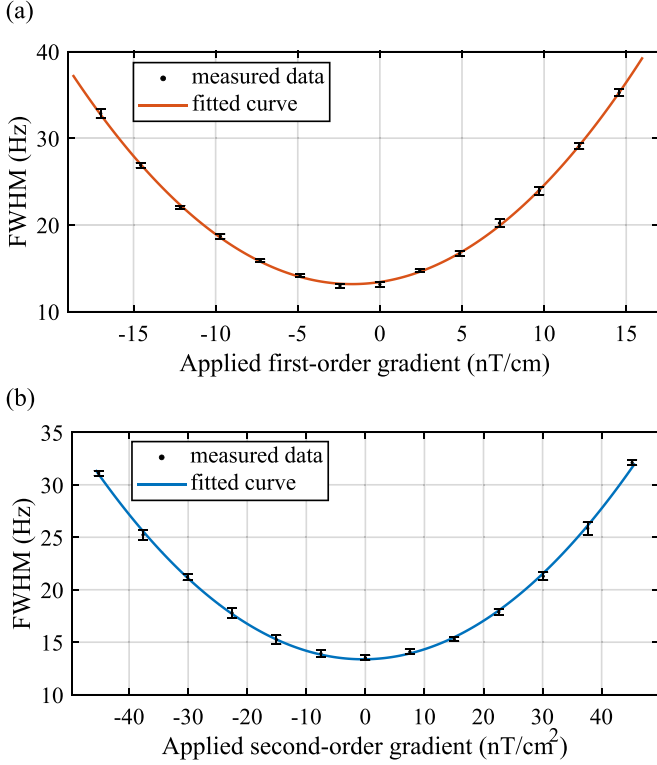


FIG. 2. Experimental results of magnetic-field-gradient-induced relaxation under  $B_0 \approx 1200$  nT. (a) Relation between the measured linewidth of the magnetic resonance and the applied first-order magnetic-field gradient ( $\partial B_z/\partial z$ ). A quadratic function (red line) is used to fit the measured data (black points). (b) Relation between the measured linewidth of the magnetic resonance and the applied second-order magnetic-field gradient ( $\partial^2 B_z/\partial z^2$ ). A quadratic function (blue line) is used to fit the measured data (black points). For each gradient, the magnetic resonance linewidth is measured for five times, through which the error bar is derived.

$T_2$  is sensitive to the axial gradient  $\partial^l B_z/\partial z^l$  generated with the coils and remains independent of the bias magnetic field [35].

Figure 2(a) illustrates the relation between the measured linewidth of the magnetic resonance and the first-order magnetic-field gradient,  $\partial B_z/\partial z$ . For each gradient, the magnetic resonance linewidth is measured for five times. The standard deviation gives the corresponding error bar. Equation (4) shows clearly that the corresponding transverse spin relaxation exhibits a quadratic dependence on  $\partial B_z/\partial z$ , which takes the form

$$\text{FWHM} = \frac{1}{\pi T_2} = a_1 \left( \frac{\partial B_z}{\partial z} - b_1 \right)^2 + \gamma_0, \quad (6)$$

where  $a_1$  is the fitted quadratic coefficient, which characterizes the response to the first-order magnetic-field gradient of the transverse spin relaxation;  $b_1$  denotes the constant residual first-order magnetic-field gradient at the position of the cell. Since  $b_1$  is a constant, it does not affect the estimation of  $a_1$ ;  $\gamma_0$  is the intrinsic relaxation caused by wall relaxation and optical power broadening. It is important to note that, even in the presence of a small amount of background gas, atoms still diffuse rapidly and pass through the beam region multiple times during the relaxation time. Hence the impact of beam

size and optical power broadening on  $a_1$  is negligible when considering the relaxation effect caused by the magnetic-field gradient in our coated cell [43].

Special attention should be given to the quadratic coefficient  $a_1$  since it is associated with the diffusion coefficient  $D$ . To determine the value of the fitted quadratic coefficient  $a_1$  along with its uncertainty, it is necessary to consider both the errors in measured linewidths and magnetic-field gradients. A fluxgate magnetometer is applied to calibrate the current-gradient coefficients of the gradient coils. The fluxgate magnetometer is positioned near the cell position and shifted axially, and the corresponding magnetic fields generated with the gradient coils are recorded. Multiple similar measurements are performed with different currents. The current-gradient coefficients of the magnetic-field-gradient coils are thus obtained through fitting the relation between the axial positions and the axial magnetic fields. The current-gradient coefficient of the first-order gradient coil in our experiment is calibrated as  $24.28 \pm 0.06$  (nT/cm)/mA (see Appendix B 2 for details).

It is reasonable to assume that the errors in first-order magnetic-field gradients and errors in linewidths are independent. Furthermore, both errors follow normal distribution [51]. With the consideration of both errors in measured linewidths and in measured first-order magnetic-field gradients, the fitted quadratic coefficient  $a_1$  can be obtained through combining total least squares and Monte Carlo methods [52,53]. For each data set in the Monte Carlo simulation, random errors with corresponding normal distributions are added to the gradients and linewidths, respectively. Then the value of  $a_1$  is obtained through the method of total least squares (see Appendix B 3). After  $10^4$  Monte Carlo simulations, the mean value and the standard deviation of  $a_1$  are

$$a_1 = (8.35 \pm 0.12) \times 10^{-2} (\text{Hz cm}^2/\text{nT}^2), \quad (7)$$

which represents the transverse spin relaxation caused by first-order magnetic-field gradient  $\partial B_z/\partial z$ . Similarly, the measured current-gradient coefficient of the second-order gradient coil is  $0.753 \pm 0.006$  (nT/cm<sup>2</sup>)/mA. The fitted quadratic coefficient  $a_2$  shown in Fig. 2(b) is

$$a_2 = (8.80 \pm 0.15) \times 10^{-3} (\text{Hz cm}^4/\text{nT}^2), \quad (8)$$

which represents the transverse spin relaxation caused by second-order magnetic-field gradient  $\partial^2 B_z/\partial z^2$ .

### C. Determination of the diffusion coefficient

As indicated in Eqs. (4) and (5), the quadratic coefficients  $a_1$  and  $a_2$  are influenced by both the cell size and the diffusion coefficient

$$a_1 = \frac{\gamma^2}{\pi} \times W(R, L, D), \quad a_2 = \frac{\gamma^2}{\pi} \times P(R, L, D). \quad (9)$$

The detailed expressions for  $W(R, L, D)$  and  $P(R, L, D)$  can be found in Appendixes A 2 c and A 2 d. These relations are also depicted in Fig. 3(a) for the cylindrical coated cell in our experiment. Therefore, the diffusion coefficient  $D$  can be determined through numerical solution after measuring  $a_1$  and  $a_2$  experimentally.

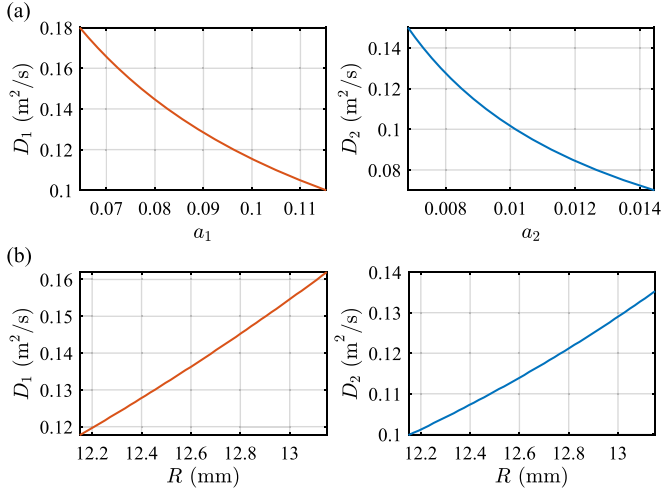


FIG. 3. Impact of quadratic coefficients and cell size on the measured diffusion coefficients. (a) The influence of  $a_1$  and  $a_2$  on the diffusion coefficients with constant cell size. (b) The influence of cell radius  $R$  on the diffusion coefficients with constant quadratic coefficients.

It should be noted that magnetic-field-gradient-induced transverse relaxation is sensitive to the cell size, as shown in Fig. 3(b); thus the measured error of cell size should be taken into consideration. The instrumental error  $\Delta = 0.02$  mm is used to represent the uncertainty of measured cell size. Considering the errors in cell size measurement and the errors in experimental fitting, the Monte Carlo simulation and numerical calculation are applied to determine the diffusion coefficients along with uncertainties based on the measured  $a_1$  and  $a_2$ , respectively, and give the values as

$$\begin{aligned} a_1 &\rightarrow D_1 = 0.137 \pm 0.002 \text{ m}^2/\text{s}, \\ a_2 &\rightarrow D_2 = 0.116 \pm 0.002 \text{ m}^2/\text{s}, \end{aligned} \quad (10)$$

where  $D_1$  and  $D_2$  denote the diffusion coefficients acquired through analyzing first-order and second-order magnetic-field-gradient-induced transverse relaxation, respectively.

#### IV. SYSTEMATIC ERRORS ANALYSIS

It is observed that there exists some deviation between the values of  $D_1$  and  $D_2$ , denoted as  $\delta D = D_1 - D_2 = 0.021 \text{ m}^2/\text{s}$ . Furthermore, the uncertainties associated with the diffusion coefficients due to cell size measurement and experimental fitting ( $\Delta D_1 \approx \Delta D_2 \approx 0.002 \text{ m}^2/\text{s}$ ) are about one order of magnitude smaller than the deviation  $\delta D$ . Hence it is necessary to analyze additional potential systematic errors contributing to  $\delta_D$ .

##### A. Cell misalignment

For an ideal situation, the cylindrical cell should be positioned at the center of the gradient coils and its axis of symmetry should be aligned along the same direction as the  $y$  axis. However, it is challenging to achieve a perfect alignment of the cell, resulting in rotational error that can impact the analysis of relaxation.

As discussed in Appendix A 3, when the cylindrical cell is positioned at the center of the gradient coils, rotation around the  $x$  axis affects the relaxation caused by magnetic-field gradients. It is assumed here that the smallest rotation error observed manually is approximately  $\Delta\alpha \lesssim 2^\circ$ . Combining coordinate transformations with numerical solutions, the two uncertainties of the diffusion coefficients caused by the rotation error can be obtained as follows:

$$\begin{aligned} \Delta\alpha \approx 2^\circ &\rightarrow \Delta D_1 \approx 0.0007 \text{ m}^2/\text{s}, \\ \Delta\alpha \approx 2^\circ &\rightarrow \Delta D_2 \approx 0.0017 \text{ m}^2/\text{s}. \end{aligned} \quad (11)$$

It is shown that the associated uncertainties are tiny ( $\Delta D_1, \Delta D_2 \ll \delta D$ ). In reality, through calibration with some horizontal references, the rotational error during the experiment should be smaller than the set value  $\Delta\alpha \approx 2^\circ$ . Therefore, the misalignment error of the cell is not the dominant contribution of  $\delta D = 0.021 \text{ m}^2/\text{s}$ .

##### B. Cell position

For a practical situation, it is also difficult to position the cell perfectly at the center of the gradient coils, resulting in displacement error that affects the analysis of relaxation. We present here a thorough analysis on displacement error of the cell in relation to the first-order gradient coil. The spatial distribution of the magnetic field generated with the first-order gradient coil can be shown as

$$B_z = \sqrt{\frac{4\pi}{3}} r Y_1^0(\theta, \phi) k_1 I = z \times k_1 I, \quad (12)$$

where  $k_1 = 24.28 \pm 0.06$  (nT/cm)/mA denotes the gradient coil coefficient and  $I$  is the current. Equation (12) shows that the first-order magnetic-field gradient experienced by the cell,  $\partial B_z / \partial z = k_1 I$ , is independent of displacement.

However, due to imperfections in the coil design, the spatial distribution of the first-order gradient is not uniform. Therefore, displacement error affects the first-order magnetic-field gradient experienced by the cell, ultimately leading to uncertainty in diffusion coefficient estimation. It is assumed here that the displacement error is about 0.5 cm. As a result, the uncertainty of the diffusion coefficient can be calculated as

$$\begin{aligned} \Delta x \approx 5 \text{ cm} &\rightarrow \Delta k_1 \rightarrow \Delta D_1 \approx 0.0006 \text{ m}^2/\text{s}, \\ \Delta y \approx 5 \text{ cm} &\rightarrow \Delta k_1 \rightarrow \Delta D_1 \approx 0.0006 \text{ m}^2/\text{s}, \\ \Delta z \approx 5 \text{ cm} &\rightarrow \Delta k_1 \rightarrow \Delta D_1 \approx 0.0012 \text{ m}^2/\text{s}. \end{aligned} \quad (13)$$

It is shown that the associated uncertainties are as well tiny ( $\Delta D_1 \ll \delta D$ ). The cell is securely fixed at the center of the first-order gradient coil through designed structural components and the actual displacement error is significantly less than the set value 0.5 cm. Consequently, the displacement error of the cell in relation to the first-order gradient coil is not the dominant contribution of  $\delta D = 0.021 \text{ m}^2/\text{s}$ .

Another examination is performed on the displacement error of the cell in relation to the second-order gradient coil. The spatial distribution of the magnetic field generated with

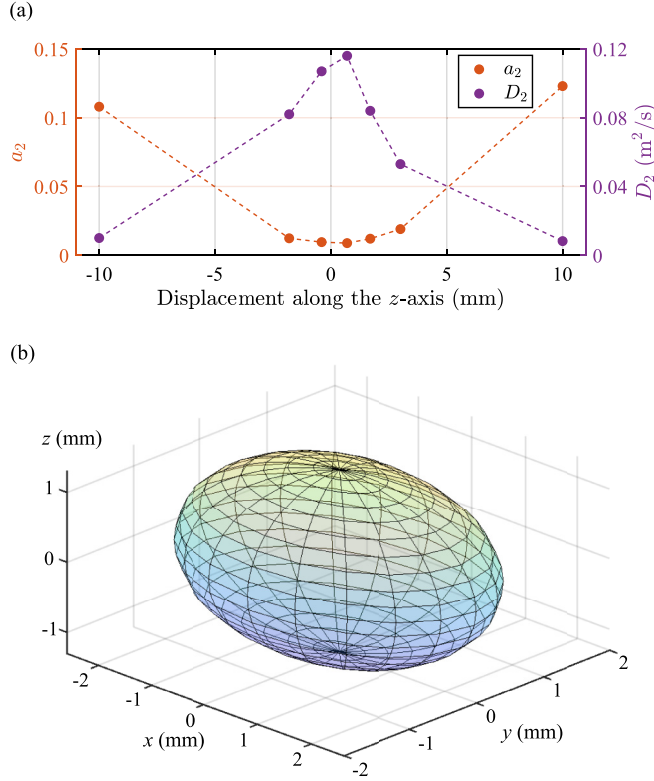


FIG. 4. Impact of the spatial displacement on measurement of diffusion coefficient  $D_2$ . (a) The influence of  $z$  displacement on  $a_2$  and  $D_2$  is measured in the experiment. The position of the detection module is manually adjusted along the  $z$  axis and the corresponding values for  $a_2$  and  $D_2$  are recorded. The cell is positioned near the center of the second-order gradient coil. Adjustments in the  $x$  and  $y$  axes are constrained by the fixed structure. (b) The  $\delta_D$ -displacement surface is calculated based on our proposed theory. In this figure,  $x$ ,  $y$ , and  $z$  denote the displacements of the cell along the three directions relative to the center of the second-order gradient coil. The origin of the coordinate system represents  $D_2 = D_1$  and at each point on this surface  $D_2 = D_1 - \delta_D$ , where  $\delta_D = 0.021 \text{ m}^2/\text{s}$ .

the second-order gradient coil can be depicted as

$$B_z = \sqrt{\frac{\pi}{5}} r^2 Y_2^0(\theta, \phi) k_2 I = \left( \frac{z^2}{2} - \frac{x^2 + y^2}{4} \right) \times k_2 I, \quad (14)$$

where  $k_2 = 0.753 \pm 0.006 \text{ (nT/cm}^2\text{)/mA}$  denotes the gradient coil coefficient;  $x$ ,  $y$ , and  $z$  represent the displacements along the three directions relative to the center of the gradient coil. Due to the quadratic correlation between  $B_z$  and the displacement, the presence of a displacement between the atomic cell and the center of the second-order gradient coil introduces an additional first-order magnetic-field gradient. This additional gradient can induce extra transverse relaxation. Under this condition, the quadratic coefficient  $a_2$  increases, resulting in a smaller corresponding  $D_2$  deduced by  $a_2$ . In other words, the experimental measured result of  $D_2$  is sensitive to the nonzero displacement between the atomic cell and the center of the second-order gradient coil. Figure 4(a) shows the influence of  $z$  displacement on the experimental measurement of  $D_2$ . To ensure the accuracy of the experiment, the coated cell should be positioned at the center of the second-order

gradient coil. Under this condition, the measured  $a_2$  is at the most accurate and the minimum level. The measured  $a_2$  in Eq. (8) represents the minimum result achievable through manual adjustments on the axial displacement of the detection module. However, the corresponding diffusion coefficient  $D_2$  is still smaller than  $D_1$ .

Assuming that there is an optimal placement of the atomic cell where  $D_2$  equals  $D_1$ , then a  $\delta_D$ -displacement surface can be employed to depict the relation between the displacement and the deviation  $\delta_D$ . The  $\delta_D$ -displacement surface is illustrated in Fig. 4(b), where the origin of the coordinate system means  $\delta_D = D_1 - D_2 = 0$  and, at each point on this surface,  $\delta_D = 0.021 \text{ m}^2/\text{s}$ . It can be observed that the boundary of axial displacement corresponding to the  $\delta_D$ -displacement surface is approximately 1 mm. Given that  $\delta_D$  is also sensitive to displacements along the  $x$  axis and  $y$  axis, performing fine manual adjustments becomes challenging. Therefore, it is reasonable to conclude that the displacement error of the cell in relation to the second-order gradient coil is the dominant factor contributing to  $\delta D = 0.021 \text{ m}^2/\text{s}$ .

### C. Coil imperfections

Imperfections in the coil design may also introduce additional errors. For the first-order gradient coil, the generated magnetic-field gradient includes not only the first-order component but also higher-order components. Hence, as mentioned above, the imperfection in design of the first-order gradient coil is similar to a displacement problem of the cell and is not the dominant factor of  $\delta D = 0.021 \text{ m}^2/\text{s}$ . Similarly, there will be additional tiny first-order gradients generated with the second-order gradient coil. However, as we discussed earlier, the relative displacement between the cell and the center of the second-order gradient coil as well causes the cell to experience an additional first-order gradient. In other words, the imperfection in design of the second-order gradient coil can be equated to a displacement problem of the cell.

In conclusion, after analyzing the impact of various errors independently, it can be determined that the deviation,  $\delta D = 0.021 \text{ m}^2/\text{s}$ , primarily originates from the displacement of the cell relative to the center of the second-order gradient coil, as summarized in Table I. It is also credible to assume that there exists an ideal position for the cell where  $\delta D = D_1 - D_2 \approx 0$ , which means that the diffusion coefficient measured by the proposed method is about  $0.137 \text{ m}^2/\text{s}$ . Considering that the measurement result error is more sensitive to the displacement and/or misalignment error from the second-order magnetic-field-gradient coil, we adopt the measured diffusion coefficient based on using the first-order magnetic-field-gradient coil as the final result. This result is consistent with the order of magnitude reported in pioneering studies of coated cells with background gas [24,33].

## V. DISCUSSION

### A. Pressure of the background gas

In this work, the magnetic-field-gradient-induced spin relaxation is analyzed to determine the diffusion coefficient for potassium atoms in the background gas within a cylindrical paraffin-coated cell. The corresponding diffusion coefficient

TABLE I. Summary of potential systematic errors in diffusion coefficient measurements.  $\Delta R$  and  $\Delta L$  represent errors in cell size measurements,  $\Delta a_1$  and  $\Delta a_2$  represent errors in experimental fitting,  $\Delta\alpha$  means rotational (misalignment) errors of the cell, and  $\Delta z$  means displacement errors of the cell.

Source of error	Uncertainty	$\Delta D_1$	$\Delta D_2$
Cell size measurements and data fitting	$\Delta R, \Delta L, \Delta a_1, \Delta a_2$	$\sim 0.002 \text{ m}^2/\text{s}$	$\sim 0.002 \text{ m}^2/\text{s}$
Rotation of the cell	$\Delta\alpha \approx 2^\circ$	$\sim 0.0007 \text{ m}^2/\text{s}$	$\sim 0.0017 \text{ m}^2/\text{s}$
Displacement of the cell	$\Delta z \approx 1 \text{ mm}$	$\sim 0.0002 \text{ m}^2/\text{s}$	$\sim 0.02 \text{ m}^2/\text{s}$

is obtained as  $0.137 \text{ m}^2/\text{s}$ . As discussed in our previous work, a potential application of measuring the diffusion coefficient is to evaluate the pressure of the background gas within the coated cell [43].

Based on the classical kinetic theory, the relation between diffusion coefficient and mean free path can be expressed as  $D = \lambda \bar{v}/6$  in a three-dimensional random walk, where  $\bar{v}$  is the thermal velocity of potassium atoms. With the consideration of background gas, the mean free path and diffusion coefficient are given by

$$\lambda = \frac{k_B T \bar{v}}{p_b \sigma_c v_{\text{rel}}}, \quad D = \frac{k_B T \bar{v}^2}{6 p_b \sigma_c v_{\text{rel}}}, \quad (15)$$

where  $v_{\text{rel}}$  is the mean relative velocity between potassium atoms and background gas molecules,  $T$  is the temperature of the cell,  $k_B$  is the Boltzmann constant,  $p_b$  is the pressure of the background gas, and  $\sigma_c$  is the cross section for velocity-changing collisions between the potassium atom and background gas. Hence, once the diffusion coefficient is measured, the knowledge of the cross section  $\sigma_c$  allows us to deduce the pressure of the background gas.

Theoretical calculation of the cross section  $\sigma_c$  is challenging due to the necessity of precise interaction potentials in quantum scattering theory [54,55]. Therefore, the cross section is primarily obtained through experimental measurements. The typical value of  $\sigma_c$  for the alkali-metal atoms and background gas molecules is chosen as  $\sim 1 \times 10^{-18} \text{ m}^2$  based on previous work [24,33,43]. Actually, the selection of  $\sigma_c$  depends on the composition of the background gas inside the coated cell. To the best of our knowledge, in-depth research on the composition of background gas inside potassium vapor cells coated with paraffin is currently insufficient. Consequently, it should be emphasized that our estimation of the background gas pressure is a relatively rough approximation.

For the alkali-metal atomic vapor cell coated with paraffin, which is typical composed of long-chain alkanes, alkali-metal atoms could undergo a chemical reaction with paraffin upon contact with the coating. The corresponding chemical reaction could lead to the breaking of the carbon chain in the paraffin, potentially producing hydrogen and hydrocarbons. Reference [23] describes an experiment in which a paraffin-coated Rb vapor cell is opened in a vacuum chamber and the released background gas is analyzed using a quadrupole mass spectrometer. The result suggests that the background gas inside the paraffin-coated Rb vapor cell is predominantly composed of hydrocarbons with three or more carbon atoms (C3 and higher), along with hydrogen.

In our fabricated coated cell, it is assumed that the primary components of the background gas are hydrogen and

hydrocarbons. Some measured cross sections between potassium atoms and various molecules are listed in Table II. Considering the diverse components of the background gas, the approximate mean values are opted for  $v_{\text{rel}} \approx 1000 \text{ m/s}$  and  $\sigma_c \approx 5 \times 10^{-18} \text{ m}^2/\text{s}$ . The pressure of background gas of our coated cell can be determined as  $p_b \approx 0.24 \text{ Pa}$ , which is significantly higher than the saturated vapor pressure of the potassium atoms ( $9.21 \times 10^{-5} \text{ Pa}$ ).

It is important to reiterate that our measurement about background gas pressure is a rough estimation, due to the complex mechanism of chemical reaction between alkali-metal atoms and the coating material, as well as the dependence of background gas composition on the type of paraffin [23]. Nevertheless, our work still introduces a potential noninvasive method for analyzing background gas pressure inside the coated cell.

## B. Performance of the coated cell

Our work provides a noninvasive method for measuring the diffusion coefficient of atoms in the background gas, as well as an estimation of background gas pressure through diffusion coefficient measurement. The measurement of these parameters facilitates further evaluation for the performance of the coated cell.

The measurement of diffusion coefficient helps directly assess the motional averaging effect. In addition to the magnetometry, the coated cell exhibiting the motional averaging effect is also employed in the development of quantum systems that require long coherence times, such as photonic networks and single-photon sources [11,12]. Consequently, measuring the diffusion coefficient is advantageous for evaluating the performance of the coated cell in practical applications.

Taking into account the saturated vapor pressure under ideal condition, the mean free path of atoms inside the coated

TABLE II. Corresponding cross sections ( $\sigma_c$ ) between potassium atoms and various molecules are experimentally determined in Refs. [56,57]. The mean relative velocities between potassium atoms and these molecules are calculated at a temperature of  $58.8^\circ\text{C}$ .

Molecule	$\sigma_c \text{ (m}^2\text{)}$	$v_{\text{rel}} \text{ (m/s)}$
K - H <sub>2</sub>	$2.36 \times 10^{-18}$	2077.9
K - CH <sub>4</sub>	$7.12 \times 10^{-18}$	850.9
K - C <sub>2</sub> H <sub>4</sub>	$9.54 \times 10^{-18}$	709.9
K - C <sub>2</sub> H <sub>6</sub>	$9.62 \times 10^{-18}$	696.0
K - C <sub>3</sub> H <sub>6</sub>	$11.52 \times 10^{-18}$	637.3
K - C <sub>3</sub> H <sub>8</sub>	$11.82 \times 10^{-18}$	630.3

cell is much larger than the cell size. The relaxation caused by the magnetic-field gradient is inversely proportional to the atomic velocity [15], which indicates that a higher velocity results in a more pronounced motional averaging effect. With the consideration of the background gas, the mean free path of atoms becomes comparable to or even smaller than the cell size. Under this condition, the motional averaging effect is more effectively characterized by the diffusion coefficient  $D$  than by the atomic velocity  $\bar{v}$ . A larger diffusion coefficient implies more rapid atomic motion, indicating a more significant motional averaging effect. Furthermore, it should be noted that, in order to guarantee the validity of our proposed method, the background gas pressure inside the cell must not be too high, so that the corresponding diffusion coefficient must not be too small.

Measuring the diffusion coefficient and estimating the background gas pressure are also advantageous for a more accurate assessment of wall-induced relaxation. The wall-induced relaxation can be represented by the longitudinal relaxation time  $T_1$ , which can be measured in experiment.  $T_1$  is related to the atomic diffusion and the number of bounces  $N$  before depolarization. In other words,  $T_1$  is closely related to the time taken by the atom to undergo  $N$  depolarization wall collisions. Therefore, a longer  $T_1$  implies a smaller wall-induced relaxation rate.

At the presence of a small amount of background gas, in the case where  $T_1 \gg R^2/D$ , due to the cluster of background gas near the cell wall, the atoms tend to hit the wall several times before diffusing away [58]. Under this condition, the presence of background gas does not affect the time taken by atoms to undergo  $N$  depolarization wall collisions. In other words, a small amount of background gas does not impact the longitudinal relaxation time  $T_1$ , i.e., the wall-induced relaxation rate [43]. However, when the background gas pressure becomes higher, wall-induced relaxation involves a more intricate mechanism and  $T_1$  is related to the diffusion coefficient of atoms [59,60]. Under this condition, the presence of background gas can influence the wall-induced relaxation.

Additionally, the measurement of diffusion coefficient and background gas pressure are beneficial for evaluating the performance of the coating. The background gas is generated through the chemical reaction between alkali-metal atoms and the coating. On the one hand, this chemical reaction may have positive effects on the coating. Some previous experiments indicate that the wall-induced relaxation rate decreases after alkali-metal atoms react with the coating [19,20]. Reference [20] indicates that chemical reactions with Rb atoms remove residual silanol groups (Si-OH) from the wall surface. This process leads to a more uniform coverage of the surface with methyl -CH<sub>3</sub> groups, which could be a potential factor contributing to the enhancement of coating properties. On the other hand, the chemical reaction also generates compounds of alkali metal, which may act as impurities adhering to the coating surface and thus affect the performance of the coating [20]. Thus the measurement of the background gas pressure becomes beneficial for evaluating the performance of the coating and provides a feasible approach for analyzing the degree of chemical reaction between the coating and alkali-metal atoms.

## VI. CONCLUSIONS AND OUTLOOK

With the consideration of non-negligible background gas, the diffusion coefficient of potassium atoms in a cylindrical paraffin-coated cell is determined by analyzing the transverse spin relaxation caused by first-order and second-order magnetic-field gradients, due to the distinct dependencies of these two relaxation effects on the diffusion coefficient. Our experiment shows that there is a deviation between the two measured values, denoted as  $\delta D$ . Further error analysis reveals that this deviation mainly arises from the relative displacement between the cell and the center of the second-order gradient coil. Based on detailed calculations, it can be found that the deviation  $\delta D$  corresponds to a cell displacement error of approximately 1 mm. Considering the precision of manual adjustments, it is determined that the measured deviation falls within the estimated error range. Ultimately, it is reasonable to adopt the value of  $0.137 \text{ m}^2/\text{s}$  as the diffusion coefficient of potassium atoms in background gas, indicating an estimated background gas pressure at approximately 0.25 Pa. This pressure is significantly higher than the saturated vapor pressure of alkali-metal atoms. Our study offers a potential guidance to determine the background gas pressure nondestructively, facilitates a more complete evaluation on the performance of the coated cell, and is of crucial importance for promoting the applications of coated vapor cells in high-sensitivity magnetometry in challenging environments.

## ACKNOWLEDGMENTS

The authors acknowledge the insightful comments and suggestions from the anonymous reviewers for improving the readability of the manuscript. This work is supported by the National Natural Science Foundation of China (Grant No. 62071012) and the National Hi-Tech Research and Development (863) Program. T.W. acknowledges the support from the start-up funding for young researchers of Peking University.

## APPENDIX A: THEORETICAL MODEL

### 1. Spherical harmonic expansion of magnetic field

This section introduces the relation between the magnetic field and magnetic-field gradient  $\partial^l B_z / \partial z^l$ . According to the classical electromagnetic theory, the magnetic field experienced by the cell can be represented by the scalar potential

$$\vec{B} = -\nabla\varphi. \quad (\text{A1})$$

The scalar potential satisfies Laplace's equation,  $\nabla^2\varphi = 0$ , and the corresponding general solution takes the form

$$\varphi = -\sum_{lm} B_l^m \frac{\sqrt{4\pi}}{l! \sqrt{2l+1}} r^l Y_l^m(\theta, \phi), \quad (\text{A2})$$

where  $Y_l^m(\theta, \phi)$  is the spherical harmonic with  $l$  and  $m$ ;  $B_l^m$  represents the weight of the corresponding component in  $\vec{B}$ . Based on Eqs. (A1) and (A2), the magnetic field could be arranged as [61]

$$\vec{B} = \sum_{lm} B_l^m \frac{\sqrt{4\pi}}{l!} r^{l-1} \vec{Y}_{j=l,m}^{l-1,1}(\theta, \phi). \quad (\text{A3})$$



Here,  $\bar{Y}_{j=l,m}^{l-1,1}(\theta, \phi)$  is the vector spherical harmonic [62]

$$\bar{Y}_{j=l,m}^{l-1,1}(\theta, \phi) = \sum_{m', \sigma} \langle l-1, m'; 1, \sigma | j=l, m \rangle Y_{l-1}^{m'}(\theta, \phi) \bar{e}_\sigma, \quad (\text{A4})$$

where  $\langle l-1, m'; 1, \sigma | j=l, m \rangle$  is the Clebsch-Gordan coefficient and  $\bar{e}_\sigma$  is the spherical unit vector. Therefore, the longitudinal component of the magnetic field is

$$B'_z \bar{e}_z = \sum_{lm} B_l^m \frac{\sqrt{4\pi l}}{l!} r^{l-1} \langle l-1, m; 1, 0 | l, m \rangle Y_{l-1}^m(\theta, \phi) \bar{e}_z, \quad (\text{A5})$$

where the constant  $B_l^m$  represents the gradient components with different orders. If  $l=1$ , then only  $m=0$  holds;  $B_1^0$  means the uniform component of  $B'_z$ . If  $l=2$ , then  $m=0, \pm 1$  holds and  $B_2^m$  means the three independent first-order gradient components corresponding to  $B'_z$  and can be denoted as  $\partial B'_z / \partial x$ ,  $\partial B'_z / \partial y$ , and  $\partial B'_z / \partial z$ . If  $l=3$ , then  $m=0, \pm 1, \pm 2$  holds and  $B_3^m$  means the five independent second-order gradient components corresponding to  $B'_z$ . Consequently, Eq. (A5)

illustrates how the axial magnetic field is expanded in terms of magnetic-field gradients.

Since the coils used in the experiment exhibit rotational symmetry about the  $z$  axis, the axial magnetic field  $B'_z$  generated with the coils also exhibits azimuthal symmetry. By setting  $m=0$ , the spherical harmonic  $Y_{l-1}^m(\theta, \phi)$  in Eq. (A5) becomes independent of  $\phi$  and  $B'_z$  transforms into an azimuthally symmetrical field:

$$\begin{aligned} B'_z &= \sum_{l=1} B_l^0 \frac{\sqrt{4\pi l}}{l!} r^{l-1} \langle l-1, 0; 1, 0 | l, 0 \rangle Y_{l-1}^0(\theta, \phi) \\ &= \sum_{l=0} B_{l+1}^0 \frac{1}{l!} \sqrt{\frac{4\pi}{2l+1}} r^l Y_l^0(\theta, \phi). \end{aligned} \quad (\text{A6})$$

It can be observed that the constant  $B_{l+1}^0$  corresponds to the zonal magnetic-field gradient  $\partial^l B_z / \partial z^l$ :

$$B'_z = \sum_{l=0} \frac{\partial^l B_z}{\partial z^l} \frac{1}{l!} \sqrt{\frac{4\pi}{2l+1}} r^l Y_l^0(\theta, \phi). \quad (\text{A7})$$

Finally,  $B'_z$  can be expressed as an expansion of zonal magnetic-field gradient  $\partial^l B_z / \partial z^l$  with the spherical harmonic

$$\begin{aligned} B'_z(x, y, z) &= B_1^0 + r Y_1^0(\theta, \phi) \sqrt{\frac{4\pi}{3}} \frac{\partial B_z}{\partial z} + r^2 Y_2^0(\theta, \phi) \sqrt{\frac{\pi}{5}} \frac{\partial^2 B_z}{\partial z^2} + r^3 Y_3^0(\theta, \phi) \frac{1}{3} \sqrt{\frac{\pi}{7}} \frac{\partial^3 B_z}{\partial z^3} \dots \\ &= B_1^0 + r \cos \theta \frac{\partial B_z}{\partial z} + \frac{r^2}{4} (3 \cos^2 \theta - 1) \frac{\partial^2 B_z}{\partial z^2} + \frac{r^3}{12} (5 \cos^3 \theta - 3 \cos \theta) \frac{\partial^3 B_z}{\partial z^3} \dots \\ &= B_1^0 + z \frac{\partial B_z}{\partial z} + \left( \frac{z^2}{2} - \frac{x^2 + y^2}{4} \right) \frac{\partial^2 B_z}{\partial z^2} + \left( \frac{5z^3}{12} - \frac{zr^2}{4} \right) \frac{\partial^3 B_z}{\partial z^3} \dots, \end{aligned} \quad (\text{A8})$$

where  $B_1^0$  is the uniform component of the magnetic field;  $(x, y, z)$  and  $(r, \theta, \phi)$  represent the positions in Cartesian coordinates and spherical coordinates, respectively. Based on Eq. (A8), it can be deduced that any arbitrary azimuthally symmetrical field  $B'_z(x, y, z)$  generated with the coils can be expressed in terms of zonal magnetic-field gradients. The expansion coefficient associated with displacement represents the spatial distribution mode of the corresponding constant  $\partial^l B_z / \partial z^l$ . For the uniform field  $B_0$ , the corresponding gradient components are zero, indicating that the magnetic field does not vary spatially.

## 2. Redfield theory with Langevin's diffusion equation

### a. Redfield theory

In the Redfield theory, the relaxation of spin polarization caused by magnetic-field gradient can be represented through the power spectral density of the magnetic-field perturbation, along with the longitudinal relaxation time  $T_1$  and the transverse relaxation time  $T_2$  [36,43],

$$\begin{aligned} \frac{1}{T_1} &= \frac{\gamma^2}{2} [S_{1x}(\omega_0) + S_{1y}(\omega_0)], \\ \frac{1}{T_2} &= \frac{1}{2T_1} + \frac{\gamma^2}{2} S_{1z}(0), \end{aligned} \quad (\text{A9})$$

where

$$S_{1x,y,z}(\omega) = \int_{-\infty}^{+\infty} \langle B_{1x,y,z}(\vec{r}, t) B_{1x,y,z}(\vec{r}, t + \tau) \rangle e^{-i\omega\tau} d\tau \quad (\text{A10})$$

are the power spectral density of magnetic-field perturbation  $B_{1x,y,z}(\vec{r}, t)$ .  $\langle \dots \rangle$  means the ensemble average,  $\gamma$  is the gyro-magnetic ratio, and  $\omega_0 = \gamma B_0$  is the atomic spin precession frequency under the bias magnetic field  $B_0$ , which is assumed to be along the  $z$  axis.

More specifically, the total magnetic field experienced by the atoms can be denoted as  $B = B_0 + B_{1x,y,z}(\vec{r}, t)$ , where  $B_0$  denotes the uniform component and  $B_{1x,y,z}(\vec{r}, t)$  represents the nonuniform magnetic-field perturbation along the  $x$ ,  $y$ , and  $z$  axes, respectively. The perturbation  $B_{1x,y,z}(\vec{r}, t)$  is related to the influence of the magnetic-field gradient on the atoms. In this work, the primary goal is on the impact of the axial perturbation  $B_{1z}(\vec{r}, t)$  on transverse spin relaxation. The magnetic-field perturbation itself does not change over time. However, due to the rapid atomic motion within the cell,  $B_{1x,y,z}(\vec{r}, t)$  experienced by an atom varies at different moments. Redfield theory requires that the impact of magnetic-field perturbation on the evolution of spin polarization is small. Based on Eqs. (A9) and (A10), the spin relaxation problem is simplified to determining the correct

form of the autocorrelation function of magnetic-field perturbation, denoted as  $\langle B_{1x,y,z}(\vec{r}, t) \cdot B_{1x,y,z}(\vec{r}, t + \tau) \rangle$ .

Taking the first-order magnetic-field gradient as an example, autocorrelation function of magnetic-field perturbation takes the form

$$\langle B_{1i}(t) \cdot B_{1i}(t + \tau) \rangle = |\nabla B_{1i}|^2 \langle i(t)i(t + \tau) \rangle, \quad i = x, y, z, \quad (\text{A11})$$

$$\langle i(t)i(t + \tau) \rangle = \langle i(t_0 + \tau)i(t_0) \rangle = \iint \rho(\vec{r}_0, t_0) \rho(\vec{r}, t_0 + \tau | \vec{r}_0, t_0) i(t_0 + \tau) i(t_0) d\Omega d\Omega_0, \quad (\text{A12})$$

the integration boundaries of  $d\Omega$  and  $d\Omega_0$  are determined by the shape and size of the cell, and  $\rho(\vec{r}_0, t_0) = 1/V$  is a uniform initial probability density for the cell with volume  $V$ . The term  $\rho(\vec{r}, t | \vec{r}_0, t_0)$  in Eq. (A12) represents the conditional probability density of an atom being at position  $\vec{r}$  at time  $t$ , given that its initial time and position are  $t_0$  and  $\vec{r}_0$ , respectively. Therefore, our problem is reduced to finding the correct expression for the conditional probability density  $\rho(\vec{r}, t | \vec{r}_0, t_0)$ .

### b. Solution of Langevin's diffusion equation

Based on Langevin's diffusion equation, the evolution of the conditional probability density satisfies [43]

$$\frac{\partial}{\partial t} \rho(\vec{r}, t | \vec{r}_0, t_0) = D(1 - e^{-|t-t_0|/\tau_D}) \nabla^2 \rho(\vec{r}, t | \vec{r}_0, t_0). \quad (\text{A13})$$

Here,  $\tau_D = Dm/(k_B T)$ , in which  $m$  is the mass of a single atom,  $T$  is the temperature of the cell, and  $k_B$  is the Boltzmann constant. For a cylindrical cell with its axis aligned along the  $y$  axis, Langevin's diffusion equation can be solved in cylindrical coordinates

$$z = r \cos \theta, \quad x = r \sin \theta. \quad (\text{A14})$$

The initial condition and the boundary condition of Langevin's diffusion equation are

$$\rho(\vec{r}, t | \vec{r}_0, t_0) = \delta(\vec{r} - \vec{r}_0) = \frac{1}{r} \delta(y - y_0) \delta(r - r_0) \delta(\theta - \theta_0), \quad (\text{A15})$$

$$\rho(\vec{r}, t | \vec{r}_0, t_0)|_{r=0} < \infty, \quad \frac{\partial}{\partial r} \rho(\vec{r}, t | \vec{r}_0, t_0) \Big|_{r=R} = 0. \quad (\text{A16})$$

Here, the solution of Eq. (A13) is defined as [36]

$$\rho_{\text{total}} = \rho_c \rho_y. \quad (\text{A17})$$

The first part of Eq. (A17), denoted as  $\rho_c$ , corresponds to the solution of the cylindrical component

$$\rho_c = \frac{1}{2\pi R^2} \sum_{n,k} A_{nk} J_n\left(\frac{x_{nk}}{R} r\right) J_n\left(\frac{x_{nk}}{R} r_0\right) \times \exp[in(\theta - \theta_0)] F\left(\frac{x_{nk}^2 D}{R^2}, \tau\right), \quad (\text{A18})$$

where  $\tau = |t - t_0|$ ,  $R$  is the radius of the cylindrical cell,  $x_{nk}$  is the zero of the first derivative of the Bessel function  $J_n(x)$ ,

where  $\nabla B_{1i}$  represents the first-order of the magnetic-field gradient,  $i(t)$  means the position of an atom at the moment  $t$ , and  $\langle i(t)i(t + \tau) \rangle$  represents the autocorrelation function of the position along the  $i$  axis.  $\langle i(t)i(t + \tau) \rangle$  can be derived from the conditional probability density, providing insights into the characteristic of atomic motion

and  $A_{nk}$  has the form

$$A_{nk} = \frac{R^2}{\int_0^R r J_{nk}^2(x_{nk} r/R) dr} = \frac{2x_{nk}^2}{J_n^2(x_{nk})(x_{nk}^2 - n^2)}. \quad (\text{A19})$$

The second part of Eq. (A17), denoted as  $\rho_y$ , corresponds to the solution for the parallel plates component

$$\rho_y = \frac{1}{L} + \frac{2}{L} \sum_{n=1,3,\dots} \sin \frac{n\pi y}{L} \sin \frac{n\pi y_0}{L} F\left(\frac{n^2 \pi^2 D}{L^2}, \tau\right) + \frac{2}{L} \sum_{n=2,4,\dots} \cos \frac{n\pi y}{L} \cos \frac{n\pi y_0}{L} F\left(\frac{n^2 \pi^2 D}{L^2}, \tau\right), \quad (\text{A20})$$

where  $L$  is the length of cell, and the function  $F(\alpha, \tau)$  is defined as

$$F(\alpha, \tau) = \exp\left\{-\alpha\left[\tau + \tau_D\left(e^{-\frac{\tau}{\tau_D}} - 1\right)\right]\right\}. \quad (\text{A21})$$

### c. Transverse relaxation caused by a first-order magnetic-field gradient

With the consideration of a first-order magnetic-field gradient generated with the gradient coil, the magnetic-field perturbation takes the form

$$B_{1z}(x, y, z) = z \frac{\partial B_{1z}}{\partial z} = r \cos \theta \frac{\partial B_{1z}}{\partial z}. \quad (\text{A22})$$

Here, it is assumed that the gradient  $\partial B_{1z}/\partial z$  does not vary with space. The corresponding autocorrelation function of the magnetic-field perturbation is

$$\langle B_{1z}(t) \cdot B_{1z}(t_0) \rangle = \frac{1}{\pi R^2} \iint \left( r \cos \theta \frac{\partial B_{1z}}{\partial z} \right) \times \left( r_0 \cos \theta_0 \frac{\partial B_{1z}}{\partial z} \right) \rho_c r r_0 d\theta d\theta_0. \quad (\text{A23})$$

As for the angular integrals, only the terms with  $n = \pm 1$  remain; Eq. (A23) can be written as

$$\langle B_{1z}(t) \cdot B_{1z}(t_0) \rangle = R^2 \left( \frac{\partial B_{1z}}{\partial z} \right)^2 \sum_k A_{1k} C_k F\left(\frac{x_{1k}^2 D}{R^2}, \tau\right), \quad (\text{A24})$$

where

$$C_k = \frac{1}{R^6} \left[ \int_0^R r^2 J_1\left(\frac{x_{1k}}{R} r\right) dr \right]^2 = \frac{J_1^2(x_{1k})}{x_{1k}^4}. \quad (\text{A25})$$

The transverse relaxation time  $T_2$  can be obtained from the Redfield theory

$$\begin{aligned} \frac{1}{T_2} &= \gamma^2 \int_0^{+\infty} \langle B_{1z}(t_0 + \tau) \cdot B_{1z}(t_0) \rangle d\tau \\ &= \gamma^2 R^2 \left( \frac{\partial B_{1z}}{\partial z} \right)^2 \sum_k A_{1k} C_k \int_0^{+\infty} F \left( \frac{x_{1k}^2 D}{R^2}, \tau \right) d\tau. \end{aligned} \quad (\text{A26})$$

The exact result of the above integral requires numerical calculation. Here the impact of  $T_1$  on  $T_2$  is neglected with a large bias magnetic field  $B_0$  [35].

#### *d. Transverse relaxation caused by a second-order magnetic-field gradient*

With the consideration of the second-order magnetic-field gradient, the magnetic field takes the form

$$B_{1z} = \left[ \frac{r^2}{4} (3 \cos^2 \theta - 1) - \frac{y^2}{4} \right] \frac{\partial^2 B_{1z}}{\partial z^2}. \quad (\text{A27})$$

Similarly, the autocorrelation function of magnetic-field perturbation could be written as

$$\begin{aligned} \langle B_{1z}(t) \cdot B_{1z}(t_0) \rangle &= \left( \frac{\partial^2 B_{1z}}{\partial z^2} \right)^2 \frac{R^4}{2\pi^2} \sum_k \left[ H_{0k} F \left( \frac{x_{0k}^2 D}{R^2}, \tau \right) + 2H_{2k} F \left( \frac{x_{2k}^2 D}{R^2}, \tau \right) \right] \\ &\quad + \left( \frac{\partial^2 B_{1z}}{\partial z^2} \right)^2 \left[ \frac{L^4}{2304} + \sum_{n_y=2,4,\dots}^{\infty} \left( \frac{L^4}{2n_y^4 \pi^4} \right) F \left( \frac{n_y^2 \pi^2 D}{L^2}, \tau \right) \right], \end{aligned} \quad (\text{A28})$$

where  $H_{0k}$  and  $H_{2k}$  are given by

$$H_{0k} = \left( \frac{\pi}{4} \right)^2 A_{0k} \frac{1}{R^8} \left[ \int_0^R r^3 J_0 \left( \frac{x_{0k} r}{R} \right) dr \right]^2, \quad (\text{A29})$$

$$H_{2k} = \left( \frac{3\pi}{8} \right)^2 A_{2k} \frac{1}{R^8} \left[ \int_0^R r^3 J_2 \left( \frac{x_{2k} r}{R} \right) dr \right]^2. \quad (\text{A30})$$

Neglecting the terms which are independent of time, the transverse relaxation time can be written as

$$\begin{aligned} \frac{1}{T_2} &= \gamma^2 \int_0^{+\infty} \langle B_{1z}(t_0 + \tau) \cdot B_{1z}(t_0) \rangle d\tau \\ &= \frac{\gamma^2 R^4}{2\pi^2} \left( \frac{\partial^2 B_{1z}}{\partial z^2} \right)^2 \sum_k \left[ H_{0k} \int_0^{+\infty} F \left( \frac{x_{0k}^2 D}{R^2}, \tau \right) d\tau + 2H_{2k} \int_0^{+\infty} F \left( \frac{x_{2k}^2 D}{R^2}, \tau \right) d\tau \right] \\ &\quad + \frac{\gamma^2 L^4}{2\pi^4} \left( \frac{\partial^2 B_{1z}}{\partial z^2} \right)^2 \sum_{n_y=2,4,\dots}^{\infty} n_y^{-4} \int_0^{+\infty} F \left( \frac{n_y^2 \pi^2 D}{L^2}, \tau \right) d\tau. \end{aligned} \quad (\text{A31})$$

Combining the Redfield theory with Langevin's diffusion equation, the transverse relaxation time  $T_2$  caused by first-order magnetic-field gradient  $\partial B_{1z}/\partial z$  and second-order magnetic-field gradient  $\partial^2 B_{1z}/\partial z^2$  can be expressed as

$$\frac{1}{\pi T_2} = \frac{\gamma^2}{\pi} W(R, L, D) \times \left( \frac{\partial B_{1z}}{\partial z} \right)^2, \quad (\text{A32})$$

$$\frac{1}{\pi T_2} = \frac{\gamma^2}{\pi} P(R, L, D) \times \left( \frac{\partial^2 B_{1z}}{\partial z^2} \right)^2. \quad (\text{A33})$$

The exact results of the quadratic coefficients, i.e.,  $W(R, L, D)$  and  $P(R, L, D)$ , require numerical calculations. The forms of the corresponding quadratic coefficients are summarized as below:

$$\begin{aligned} W(R, L, D) &= R^2 \sum_k A_{1k} C_k \int_0^{+\infty} F \left( \frac{x_{1k}^2 D}{R^2}, \tau \right) d\tau, \\ P(R, L, D) &= \frac{R^4}{2\pi^2} \sum_k \left[ H_{0k} \int_0^{+\infty} F \left( \frac{x_{0k}^2 D}{R^2}, \tau \right) d\tau + 2H_{2k} \int_0^{+\infty} F \left( \frac{x_{2k}^2 D}{R^2}, \tau \right) d\tau \right] \\ &\quad + \frac{L^4}{2\pi^4} \sum_{n_y=2,4,\dots}^{\infty} n_y^{-4} \int_0^{+\infty} F \left( \frac{n_y^2 \pi^2 D}{L^2}, \tau \right) d\tau. \end{aligned} \quad (\text{A34})$$

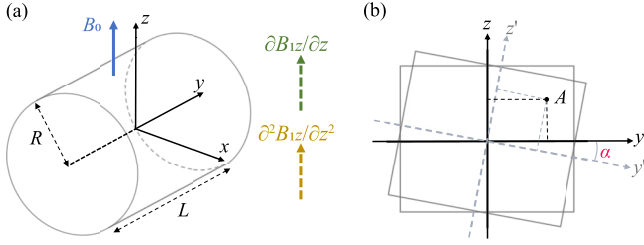


FIG. 5. Alignment and rotation of the cylindrical coated cell. (a) Three-dimensional schematic diagram of the cylindrical cell. The axis of symmetry of the cell extends along the  $y$  axis, perpendicular to the direction of the bias magnetic field  $B_0$ . (b) Schematic diagram of the cross section of the cylindrical cell in the  $zOy$  plane. The cylindrical coated cell rotates around the  $x$  axis by an angle  $\alpha$ .

### 3. Impact of cell rotation on relaxation

In the experiment, the axis of symmetry of the cylindrical cell should be aligned with the  $y$  axis to ensure accurate analysis of relaxation. As illustrated in Fig. 5(a), due to the rotational symmetry around the  $y$  axis, the rotational error around this axis does not impact the relaxation measurement. Additionally, since the magnetic fields generated with the coils exhibit azimuthal symmetry (independent of  $\phi$ ), rotational error around the  $z$  axis does not impact the relaxation as well. Consequently, in an ideal situation, only the rotational error around the  $x$  axis tends to affect the relaxation caused by magnetic-field gradients. The following contents present a theoretical approach on analyzing the systematic error caused by cell rotation or misalignment.

As is shown in Fig. 5(b), it is assumed that the cylindrical coated cell rotates around the  $x$  axis by a small angle  $\alpha$ , where  $Oxyz$  is the original laboratory coordinate system and  $Ox'y'z'$  represents the new coordinate system after the rotation. The coordinates of point  $A$  in the two coordinate systems satisfy the following relation:

$$\begin{bmatrix} x' \\ y' \\ z' \end{bmatrix} = \begin{bmatrix} 1 & 0 & 0 \\ 0 & \cos \alpha & -\sin \alpha \\ 0 & \sin \alpha & \cos \alpha \end{bmatrix} \begin{bmatrix} x \\ y \\ z \end{bmatrix}. \quad (\text{A35})$$

It is possible to calculate the relaxation information after the cell rotation through the coordinate transformation represented by Eq. (A35). For the first-order magnetic-field-gradient-induced relaxation, it is necessary to analyze the transformed autocorrelation function  $\langle z'z'_0 \rangle$  in the new coordinate system, which can be calculated that

$$\begin{aligned} \langle z'z'_0 \rangle &= \langle (y \sin \alpha + z \cos \alpha)(y_0 \sin \alpha + z_0 \cos \alpha) \rangle \\ &= \cos^2 \alpha \langle zz_0 \rangle + \sin^2 \alpha \langle yy_0 \rangle, \end{aligned} \quad (\text{A36})$$

which implies that  $\langle z'z'_0 \rangle$  in the new coordinate system can be represented as a combination of  $\langle zz_0 \rangle$  and  $\langle yy_0 \rangle$  from the original laboratory coordinate system, prior to the rotation. Subsequently, the influence of rotational error on the relaxation can be deduced from the transformed autocorrelation function and the corresponding quadratic coefficient after

rotational correction is

$$a_1^{\text{real}} = a_1^{\text{ideal}} + \sin^2 \alpha (a_{1y} - a_{1z}). \quad (\text{A37})$$

The same method can also be applied to analyze the transverse relaxation caused by the second-order magnetic-field gradient and the corresponding quadratic coefficient after rotational correction can be calculated as

$$\begin{aligned} a_2^{\text{real}} &= a_2^{\text{ideal}} + \frac{9}{16} (\cos^4 \alpha - 1) a_{2r} \\ &+ \frac{3 \sin^2 \alpha}{16} (3 \sin^2 \alpha - 2) a_{2y} + \frac{9 \sin^2 2\alpha}{16} a_{2zy}, \end{aligned} \quad (\text{A38})$$

where the  $a_1^{\text{ideal}}$  and  $a_2^{\text{ideal}}$  are the coefficients calculated in the ideal case (no rotational error), and the corresponding parameters can be shown as

$$\begin{aligned} a_{1y} &= \frac{\gamma^2}{\pi} \int_0^{+\infty} \langle yy_0 \rangle d\tau, & a_{1z} &= \frac{\gamma^2}{\pi} \int_0^{+\infty} \langle zz_0 \rangle d\tau, \\ a_{2y} &= \frac{\gamma^2}{\pi} \int_0^{+\infty} \langle y^2 y_0^2 \rangle d\tau, & a_{2zy} &= \frac{\gamma^2}{\pi} \int_0^{+\infty} \langle yy_0 zz_0 \rangle d\tau, \\ a_{2r} &= \frac{\gamma^2}{\pi} \int_0^{+\infty} \langle r^2 r_0^2 \cos^2 \theta \cos^2 \theta_0 \rangle d\tau, \end{aligned} \quad (\text{A40})$$

where  $y, z, r, \theta$  mean the position of an atom at moment  $t$  and  $y_0, z_0, r_0, \theta_0$  represent the position of an atom at initial moment  $t_0$ ;  $\langle \dots \rangle$  represents the autocorrelation function defined in Eq. (A12). Further detailed results can be derived through numerical calculations.

## APPENDIX B: EXPERIMENTAL PARAMETERS AND DATA PROCESSING

### 1. Linewidth of magnetic resonance

In the experiment, the precession signal of atomic polarization is measured with a photodetector and demodulated with a lock-in amplifier (Stanford Research Systems, SR865A). The magnetic resonance is recorded as a function of modulation frequency and then the signal linewidth [full width at half maximum (FWHM)] is extracted through fitting with a Lorentzian function, which has the form

$$f(\Delta x) = \frac{a_1^2 a_2}{4\Delta x^2 + a_1^2} + a_3, \quad (\text{B1})$$

where  $\Delta x$  is the frequency detuning,  $a_1$  means the linewidth of the Lorentzian function,  $a_2$  means the amplitude of the signal, and  $a_3$  is the electric noise floor. Figure 6 shows an example about the magnetic resonance signal and its corresponding fitting curve.

### 2. Current-gradient coefficients of gradient coils

In the experiment, a fluxgate magnetometer is applied to calibrate the current-gradient coefficients of the gradient coils. The fluxgate magnetometer is positioned near the cell location and moved axially. Concurrently, the corresponding axial magnetic fields generated with the gradient coils, denoted as  $B_z$ , are recorded.

Figure 7(a) shows an example about the measurement of the first-order magnetic-field gradient generated with the

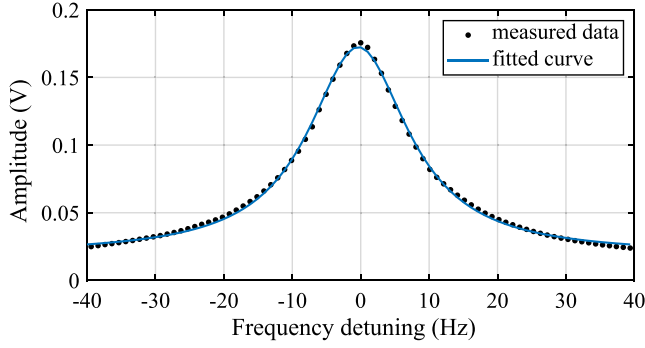


FIG. 6. Example of the magnetic resonance of our coated cell. A Lorentzian function (blue line) is used to fit the measured in-phase signal from the lock-in amplifier (black points). The corresponding linewidth of magnetic resonance is about 17.8 Hz.

first-order gradient coil. A certain current is applied to the first-order gradient coil and the corresponding axial magnetic-field distribution is measured with the fluxgate magnetometer. First-order magnetic-field gradient is characterized by the maximum slope corresponding to the center position. The current-gradient coefficient of the first-order gradient coil in our experiment is calibrated as  $24.28 \pm 0.06$  (nT/cm)/mA. Similarly, Fig. 7(b) shows an example about the measurement of the second-order magnetic-field gradient generated with the second-order gradient coil. Second-order magnetic-field gradient at the center of the coil is characterized by the corresponding quadratic coefficient

$$B_z = a \times z^2 \rightarrow \frac{\partial^2 B_z}{\partial z^2} = 2 \times a, \quad (\text{B2})$$

where  $a$  means the fitting quadratic coefficient and  $z$  means the axial position. Then, dividing the magnetic-field gradient by the coil current, the current-gradient coefficient of the second-order gradient coil is obtained. Multiple similar measurements are performed with different coil currents. The mean value and the standard deviation representing the uncertainty are recorded. The current-gradient coefficient of the second-order gradient coil in our experiment is calibrated as  $0.753 \pm 0.006$  (nT/cm<sup>2</sup>)/mA.

### 3. Data fitting with errors

In the experiment, it is necessary to fit a quadratic function to correlate the measured gradient with the magnetic resonance linewidth and record the corresponding quadratic coefficient. Due to the errors present in both the measured magnetic-field gradients and the corresponding magnetic resonance linewidths, ordinary least squares fitting cannot be directly applied. Here, the combination of total least squares fitting with the Monte Carlo simulation is employed for the fitting process [52,53].

The measured magnetic-field gradients can be represented as  $[x_1, x_2, \dots, x_i]$ , where  $x_i = \bar{x}_i \pm \sigma_{x_i}$ , and the measured linewidths can be represented as  $[y_1, y_2, \dots, y_i]$ , where  $y_i = \bar{y}_i \pm \sigma_{y_i}$ . Here,  $\sigma_{x_i}$  and  $\sigma_{y_i}$  are the corresponding errors. The proposed fitting method can be applied through the following steps.

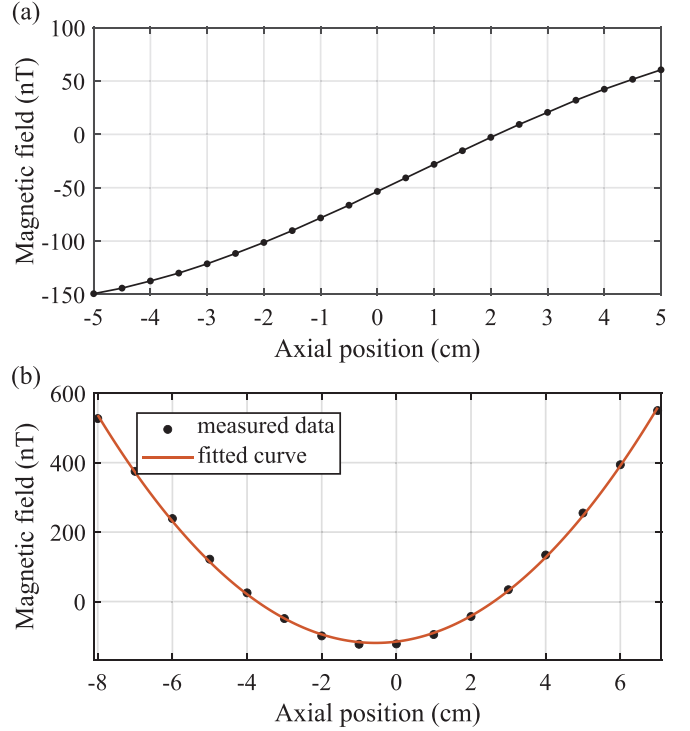


FIG. 7. Measurements of the magnetic-field gradients generated with the gradient coils. (a) The relation between the axial position and the axial magnetic field generated with the first-order gradient coil (at 1 mA). First-order magnetic-field gradient is characterized by the maximum slope corresponding to the center position. The current-gradient coefficient of the gradient coil is obtained through dividing the first-order magnetic-field gradient by the coil current. (b) The relation between the axial position and the axial magnetic field generated with the second-order gradient coil (at 32 mA). Second-order magnetic-field gradient is characterized by fitting with a quadratic function and recording the corresponding quadratic coefficient. The current-gradient coefficient of the gradient coil is obtained through dividing the second-order magnetic-field gradient by the coil current.

(1) For each data set in the Monte Carlo simulation, denoted as  $[x_1, x_2, \dots, x_i]_n$  and  $[y_1, y_2, \dots, y_i]_n$ , random errors are added to the gradients and linewidths, i.e.,  $x_i = \bar{x}_i + \delta_{x_i}$  and  $y_i = \bar{y}_i + \delta_{y_i}$ . The random errors  $\delta_{x_i}$  and  $\delta_{y_i}$  follow the corresponding normal distributions  $N(0, \sigma_{x_i})$  and  $N(0, \sigma_{y_i})$ , respectively.

(2) For each data set in the Monte Carlo simulation,  $[x_1, x_2, \dots, x_i]_n$  and  $[y_1, y_2, \dots, y_i]_n$ , the fitting quadratic coefficient  $a_n$  is obtained by the total least squares method.

(3) Repeat the simulation 10 000 times.

(4) Record the mean value of  $a_n$  and use the standard deviation to represent the uncertainty.

Through the above steps, the fitting quadratic coefficients along with uncertainties corresponding to the relaxation caused by the first-order magnetic-field gradient and the second-order magnetic-field gradient can be obtained as

$$\begin{aligned} a_1 &= (8.35 \pm 0.12) \times 10^{-2} (\text{Hz cm}^2/\text{nT}^2), \\ a_2 &= (8.80 \pm 0.15) \times 10^{-3} (\text{Hz cm}^4/\text{nT}^2). \end{aligned} \quad (\text{B3})$$

- [1] D. Budker, W. Gawlik, D. Kimball, S. Rochester, V. Yashchuk, and A. Weis, Resonant nonlinear magneto-optical effects in atoms, *Rev. Mod. Phys.* **74**, 1153 (2002).
- [2] D. Budker, V. Yashchuk, and M. Zolotarev, Nonlinear magneto-optic effects with ultranarrow widths, *Phys. Rev. Lett.* **81**, 5788 (1998).
- [3] M. Balabas, T. Karaulanov, M. Ledbetter, and D. Budker, Polarized alkali-metal vapor with minute-long transverse spin-relaxation time, *Phys. Rev. Lett.* **105**, 070801 (2010).
- [4] O. Katz and O. Firstenberg, Light storage for one second in room-temperature alkali vapor, *Nat. Commun.* **9**, 2074 (2018).
- [5] J. Sun, X. Zhang, W. Qu, E. E. Mikhailov, I. Novikova, H. Shen, and Y. Xiao, Spatial multiplexing of squeezed light by coherence diffusion, *Phys. Rev. Lett.* **123**, 203604 (2019).
- [6] R. Zhang, D. Kanta, A. Wickenbrock, H. Guo, and D. Budker, Heading-error-free optical atomic magnetometry in the earth-field range, *Phys. Rev. Lett.* **130**, 153601 (2023).
- [7] J. Jia, V. Novikov, T. B. Brasil, E. Zeuthen, J. H. Müller, and E. S. Polzik, Acoustic frequency atomic spin oscillator in the quantum regime, *Nat. Commun.* **14**, 6396 (2023).
- [8] D. Budker and M. Romalis, Optical magnetometry, *Nat. Phys.* **3**, 227 (2007).
- [9] W. Qu, S. Jin, J. Sun, L. Jiang, J. Wen, and Y. Xiao, Sub-Hertz resonance by weak measurement, *Nat. Commun.* **11**, 1752 (2020).
- [10] A. Soheilian, M. Ranjbaran, and M. M. Tehrani, Position and direction tracking of a magnetic object based on an  $M_x$ -atomic magnetometer, *Sci. Rep.* **10**, 1294 (2020).
- [11] J. Borregaard, M. Zugenmaier, J. Petersen, H. Shen, G. Vasilakis, K. Jensen, E. Polzik, and A. Sørensen, Scalable photonic network architecture based on motional averaging in room temperature gas, *Nat. Commun.* **7**, 11356 (2016).
- [12] K. B. Dideriksen, R. Schmieg, M. Zugenmaier, and E. S. Polzik, Room-temperature single-photon source with near-millisecond built-in memory, *Nat. Commun.* **12**, 3699 (2021).
- [13] Y. Xiao, M. Klein, M. Hohensee, L. Jiang, D. F. Phillips, M. D. Lukin, and R. L. Walsworth, Slow light beam splitter, *Phys. Rev. Lett.* **101**, 043601 (2008).
- [14] O. Firstenberg, M. Shuker, A. Ron, and N. Davidson, Colloquium: Coherent diffusion of polaritons in atomic media, *Rev. Mod. Phys.* **85**, 941 (2013).
- [15] S. Pustelny, D. F. Jackson Kimball, S. M. Rochester, V. V. Yashchuk, and D. Budker, Influence of magnetic-field inhomogeneity on nonlinear magneto-optical resonances, *Phys. Rev. A* **74**, 063406 (2006).
- [16] D. F. J. Kimball, J. Dudley, Y. Li, D. Patel, and J. Valdez, Constraints on long-range spin-gravity and monopole-dipole couplings of the proton, *Phys. Rev. D* **96**, 075004 (2017).
- [17] M. Bouchiat and J. Brossel, Relaxation of optically pumped Rb atoms on paraffin-coated walls, *Phys. Rev.* **147**, 41 (1966).
- [18] M. Stephens, R. Rhodes, and C. Wieman, Study of wall coatings for vapor-cell laser traps, *J. Appl. Phys.* **76**, 3479 (1994).
- [19] J. C. Camparo, Alkali ( $I \cdot S$ ) wall relaxation in dichlorodimethylsilane coated resonance cells, *J. Chem. Phys.* **86**, 1533 (1987).
- [20] J. Camparo, R. Frueholz, and B. Jaduszliwer, Alkali reactions with wall coating materials used in atomic resonance cells, *J. Appl. Phys.* **62**, 676 (1987).
- [21] Y. Yi, H. Robinson, S. Knappe, J. MacLennan, C. Jones, C. Zhu, N. Clark, and J. Kitching, Method for characterizing self-assembled monolayers as antirelaxation wall coatings for alkali vapor cells, *J. Appl. Phys.* **104**, 023534 (2008).
- [22] S. N. Atutov, R. Calabrese, A. I. Plekhanov, and L. Tomassetti, Diffusion and photodesorption of molecular gases in a polymer organic film, *Eur. Phys. J. D* **68**, 6 (2014).
- [23] A. Hatakeyama, T. Kuroda, N. Sekiguchi, and K. Ishikawa, Analysis of background gas in an alkali-metal vapor cell coated with paraffin, *Appl. Phys. B* **125**, 133 (2019).
- [24] N. Sekiguchi and A. Hatakeyama, Non-negligible collisions of alkali atoms with background gas in buffer-gas-free cells coated with paraffin, *Appl. Phys. B* **122**, 81 (2016).
- [25] E. L. Hahn, Spin echoes, *Phys. Rev.* **80**, 580 (1950).
- [26] H. Y. Carr and E. M. Purcell, Effects of diffusion on free precession in nuclear magnetic resonance experiments, *Phys. Rev.* **94**, 630 (1954).
- [27] D. C. Douglass and D. W. McCall, Diffusion in paraffin hydrocarbons, *J. Phys. Chem.* **62**, 1102 (1958).
- [28] C. Wade and J. Waugh, Temperature and pressure dependence of self-diffusion in liquid ethane, *J. Chem. Phys.* **43**, 3555 (1965).
- [29] D. W. McCall and D. C. Douglass, The effect of ions on the self-diffusion of water. I. Concentration dependence, *J. Phys. Chem.* **69**, 2001 (1965).
- [30] K. Ishikawa, Y. Anraku, Y. Takahashi, and T. Yabuzaki, Optical magnetic-resonance imaging of laser-polarized Cs atoms, *J. Opt. Soc. Am. B* **16**, 31 (1999).
- [31] K. Ishikawa and T. Yabuzaki, Diffusion coefficient and sublevel coherence of Rb atoms in  $N_2$  buffer gas, *Phys. Rev. A* **62**, 065401 (2000).
- [32] K. Ishikawa, Spin-polarized lithium diffusion in a glass hot-vapor cell, *Appl. Phys. B* **122**, 224 (2016).
- [33] Y. Tang, Y. Wen, L. Cai, and K. Zhao, Spin-noise spectrum of hot vapor atoms in an anti-relaxation-coated cell, *Phys. Rev. A* **101**, 013821 (2020).
- [34] H. C. Torrey, Bloch equations with diffusion terms, *Phys. Rev.* **104**, 563 (1956).
- [35] G. Cates, S. Schaefer, and W. Happer, Relaxation of spins due to field inhomogeneities in gaseous samples at low magnetic fields and low pressures, *Phys. Rev. A* **37**, 2877 (1988).
- [36] D. D. McGregor, Transverse relaxation of spin-polarized  $^3\text{He}$  gas due to a magnetic-field gradient, *Phys. Rev. A* **41**, 2631 (1990).
- [37] K. Hasson, G. Cates, K. Lerman, P. Bogorad, and W. Happer, Spin relaxation due to magnetic-field inhomogeneities: Quartic dependence and diffusion-constant measurements, *Phys. Rev. A* **41**, 3672 (1990).
- [38] X. Liu, C. Chen, T. Qu, K. Yang, and H. Luo, Transverse spin relaxation and diffusion-constant measurements of spin-polarized  $^{129}\text{Xe}$  nuclei in the presence of a magnetic field gradient, *Sci. Rep.* **6**, 24122 (2016).
- [39] D.-Y. Lee, S. Lee, M. Kim, and S. H. Yim, Magnetic-field-inhomogeneity-induced transverse-spin relaxation of gaseous  $^{129}\text{Xe}$  in a cubic cell with a stem, *Phys. Rev. A* **104**, 042819 (2021).
- [40] X. Zhang, J. Hu, and N. Zhao, Stable Atomic magnetometer in parity-time symmetry broken phase, *Phys. Rev. Lett.* **130**, 023201 (2023).
- [41] B. Clément, M. Guigue, A. Leredde, G. Pignol, D. Rebreyend, S. Rocchia, and S. Touati, Determination of diffusion coefficients of mercury atoms in various gases from longitudinal spin

- relaxation in magnetic gradients, *Phys. Rev. A* **106**, 062815 (2022).
- [42] R. Golub, R. M. Rohm, and C. Swank, Reexamination of relaxation of spins due to a magnetic field gradient: Identity of the Redfield and Torrey theories, *Phys. Rev. A* **83**, 023402 (2011).
- [43] J. Zheng, W. Xiao, S. Li, X. Peng, T. Wu, and H. Guo, Langevin approach to magnetic-field-gradient-induced spin relaxation in a coated cell, *Phys. Rev. A* **109**, 022803 (2024).
- [44] A. G. Redfield, On the theory of relaxation processes, *IBM J. Res. Dev.* **1**, 19 (1957).
- [45] C. P. Slichter, *Principles of Magnetic Resonance*, Springer Series in Solid-State Sciences (Springer, Heidelberg, 1990).
- [46] R. Shaham, O. Katz, and O. Firstenberg, Quantum dynamics of collective spin states in a thermal gas, *Phys. Rev. A* **102**, 012822 (2020).
- [47] W. Happer, Y.-Y. Jau, and T. Walker, *Optically Pumped Atoms* (John Wiley & Sons, Weinheim, 2010).
- [48] J. C. Robinson, *An Introduction to Ordinary Differential Equations* (Cambridge University Press, New York, 2004).
- [49] W. E. Bell and A. L. Bloom, Optically driven spin precession, *Phys. Rev. Lett.* **6**, 280 (1961).
- [50] S. J. Seltzer, *Developments in Alkali-metal Atomic Magnetometry* (Princeton University, Princeton, NJ, 2008).
- [51] P. Young, *Everything You Wanted to Know About Data Analysis and Fitting but Were Afraid to Ask* (Springer, Cham, 2015).
- [52] I. Petráš and D. Bednářová, Total least squares approach to modeling: A Matlab toolbox, *Acta Mont. Slovaca* **15**, 158 (2010).
- [53] J. Tellinghuisen, Least-squares analysis of data with uncertainty in  $x$  and  $y$ : A Monte Carlo methods comparison, *Chemom. Intell. Lab. Syst.* **103**, 160 (2010).
- [54] L. D. Landau and E. M. Lifshitz, *Quantum Mechanics: Non-Relativistic Theory* (Pergamon, Oxford, 1991).
- [55] H. Massey and R. Buckingham, Determination of van der Waals forces, *Nature (London)* **138**, 77 (1936).
- [56] E. W. Rothe and R. B. Bernstein, Total collision cross sections for the interaction of atomic beams of alkali metals with gases, *J. Chem. Phys.* **31**, 1619 (1959).
- [57] K. Lulla, H. H. Brown, and B. Bederson, Total cross sections for the scattering of potassium by He, Ne, Ar, Xe, and H<sub>2</sub> in the thermal energy range, *Phys. Rev.* **136**, A1233 (1964).
- [58] D. J. Bicout, E. I. Kats, A. K. Petukhov, and R. S. Whitney, Size independence of statistics for boundary collisions of random walks and its implications for spin-polarized gases, *Phys. Rev. Lett.* **110**, 010602 (2013).
- [59] S. J. Seltzer, D. M. Rampulla, S. Rivillon-Amy, Y. J. Chabal, S. L. Bernasek, and M. V. Romalis, Testing the effect of surface coatings on alkali atom polarization lifetimes, *J. Appl. Phys.* **104**, 103116 (2008).
- [60] S. Knappe and H. G. Robinson, Double-resonance lineshapes in a cell with wall coating and buffer gas, *New J. Phys.* **12**, 065021 (2010).
- [61] D. Sheng, A. Kabcenell, and M. V. Romalis, New classes of systematic effects in gas spin comagnetometers, *Phys. Rev. Lett.* **113**, 163002 (2014).
- [62] D. A. Varshalovich, A. N. Moskalev, and V. K. Khersonskii, *Quantum Theory of Angular Momentum* (World Scientific, Singapore, 1988).